Smart Materials and Structures

An experimental study of a semiactive magneto-rheological fluid variable damper for vibration suppression of truss structures

INSTITUTE OF PHYSICS PUBLISHING SMART MATERIALS AND STRUCTURES
Smart Mater. Struct. **11** (2002) 156–162 PII: S0964-1726(02)31568-4

An experimental study of a semiactive magneto-rheological fluid variable damper for vibration suppression of truss structures

Hyun-Ung Oh and Junjiro Onoda

The Institute of Space and Astronautical Science, Department of Space Transportation,
3-1-1 Yoshinodai, Sagamihara, Kanagawa 229-8510, Japan

Received 30 July 2001, in final form 13 November 2001
Published 6 February 2002
Online at stacks.iop.org/SMS/11/156

Abstract
The purpose of this paper is to demonstrate that vibrations of a truss structure can be suppressed nicely by a magneto-rheological (MR) fluid variable damper for semiactive vibration suppression. A variable MR fluid damper was designed and fabricated for this study. The principal characteristics of an MR damper were measured in dynamic tests, and a mathematical model of the damper was proposed. To investigate if the variable damper effectively suppresses the vibration of actual truss structures, semiactive vibration suppression experiments were performed using a cantilevered ten-bay truss beam. The experimental result has shown that the vibration was suppressed nicely by the variable MR damper, and that was compared with that of an electro-rheological (ER) damper investigated in previous research. The MR damper showed a higher performance than that of the ER damper.

1. Introduction

In a semiactive vibration suppression system, vibration is suppressed by passive energy dissipation mechanisms. Therefore, unlike an active system, a semiactive system is always stable even when the control logic is improper because of the lack of exact information about the dynamic characteristics of the structures. The vibration suppression performance of the semiactive system is also much better than that of the passive system. The effectiveness of semiactive systems for space truss structures has been reported in [1–6].

To implement semiactive vibration suppression, we need to control the state of the structural system by controlling some devices whose mechanical characteristics are variable. There are various types of such variable devices including the following devices. A semiactive variable friction system that uses piezoelectrics has been described by Onoda *et al* [1]. A semiactive stiffness system for the seismic response control of structures has been investigated by Kobori *et al* [7]. A solenoid valve type on–off semiactive fluid viscous damper has been investigated for seismic response control by Symans *et al* [8]. Semiactive systems using smart materials such as electro-rheological (ER) or magneto-rheological (MR) fluids whose characteristics can be controlled by the strength of the electric or magnetic fields have also been investigated by many researchers. The concept of using ER fluids to suppress vibration in truss structures has been studied by Onoda *et al* [3–5] and Oh *et al* [6]. Onoda *et al* [3, 4] measured the characteristics of a particle-dispersion type of ER fluid damper for semiactive vibration suppression of truss structures. Their numerical simulation and experiment results have demonstrated the effectiveness of semiactive vibration suppression. To improve the performance of the ER fluid damper of [3, 4], Onoda *et al* [5] proposed a method that exploits a high-frequency vibration of an electrode after turning off the high voltage to the electrode. They also confirmed that the proposed method reduced the amplitudes of the vibrations to a low level. Oh *et al* [6] measured the characteristics of a variable damper for semiactive vibration suppression of truss structures with a liquid-crystal type of ER fluid, which is a single-phase ER fluid. They also performed a numerical simulation to compare the effectiveness of the semiactive vibration suppression using liquid-crystal and particle-dispersion types of ER fluid damper.

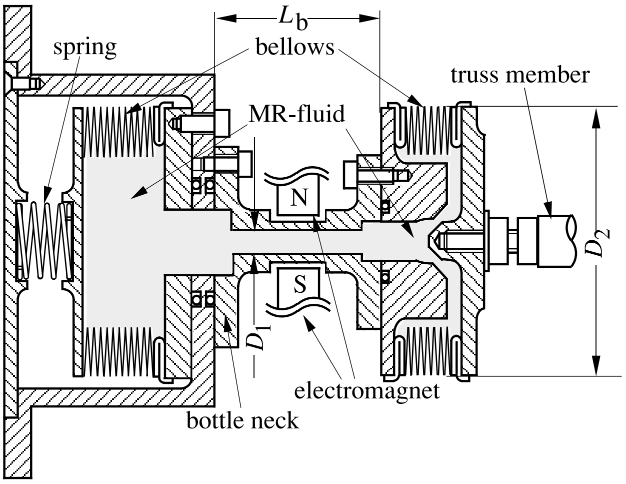

Figure 1. Cross section of a MR fluid damper ($L_b = 70$ mm, $D_1 = 6$ mm $D_2 = 40$ mm).

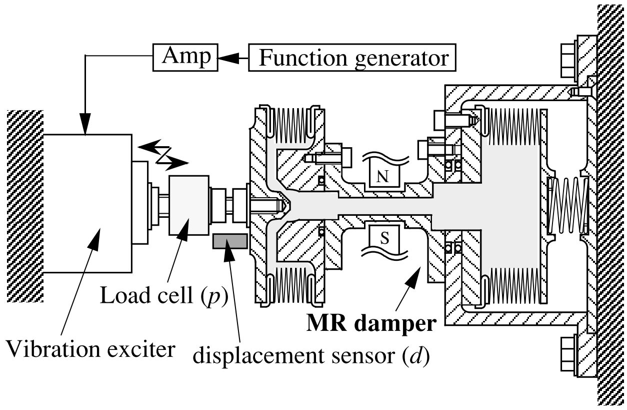

Figure 2. Experimental set-up for dynamic tests of the MR fluid damper.

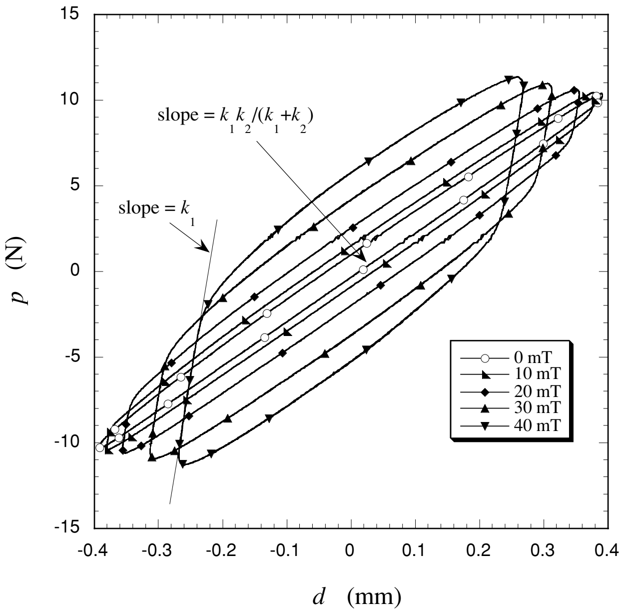

Figure 3. Elongation–load (d–p) relation measured in dynamic tests of the MR damper at various constant input magnetic fields H (exciting frequency = 0.5 Hz).

The rheological behaviour of MR fluids is similar to that of the particle-dispersion type of ER fluid [9]. However, when compared with the particle-dispersion type of ER fluid, MR fluids have superior properties in a much wider temperature range, typically −40 to 150 °C [9]. MR fluids have been used to develop vibration suppression devices [9–12]. Dyke *et al* [10] reported that a semiactive system using an MR damper is quite effective for seismic response reduction over a wide range of seismic excitations. Lee *et al* [11] demonstrated the superior performance of Lyapunov semiactive vibration control with an MR fluid actuator. Tsuchiya *et al* [12] reported on an application study of MR fluids in a small variable-damping mount intended for precision equipment of automobiles, such as CD players. Spencer *et al* [13] proposed a model that can effectively simulate the behaviour of a typical MR damper based on a Bouc–Wen hysteresis model.

In this paper, to implement semiactive vibration suppression of space truss structures, we focus on MR fluids belonging to a class of smart materials. The purposes of this research are to investigate the characteristics of an MR fluid damper, to experimentally demonstrate the effectiveness of the semiactive damper using the MR fluid and to compare the effectiveness of the semiactive vibration suppression using the MR damper and the particle-dispersion type of ER fluid damper of [3].

2. Semiactive variable damper with MR fluid

Figure 1 shows a cross section of a bellows type of MR fluid damper composed of two variable volume chambers filled with MR fluid. The structure of this damper is similar to that of the ER damper of [3] except that an electromagnet is installed to apply a magnetic field to the MR fluid in the bottleneck. The properties of the MR fluid in the bottleneck are varied when the magnetic field is applied. The MR fluid used in this study is E-600 fluid (Sigma Hi-Chemical). The electromagnet fabricated in this study generates a magnetic-flux density of 40 mT at the middle of the gap between N and S poles for an electric current of 2 A. It responds quickly to the switching on and off of the input electric current, within 3 ms, and the residual magnetic field just after switching off the input magnetic field is about 2 mT.

We performed dynamic tests of the damper to measure characteristics of the MR fluid damper. Figure 2 shows a block diagram for the dynamic tests. A sinusoidal exciting force was applied by a vibration exciter when the magnetic field H to the electromagnet was kept constant, and the load (p) on the damper and the elongation (d) of the damper were measured using a load cell and an eddy-current type of non-contact displacement sensor respectively, as shown in figure 2. Figure 3 shows some typical examples of the d–p relations measured in the dynamic tests at an exciting frequency of 0.5 Hz and various constant magnetic fields. When a high magnetic field is applied to the damper, the stiffness is high in the low-load range. However, when the load level exceeds the 'yielding' level, the stiffness becomes low, resulting in a bilinear plot. The stiffness in the load range which is larger than the 'yielding' level is almost identical with that

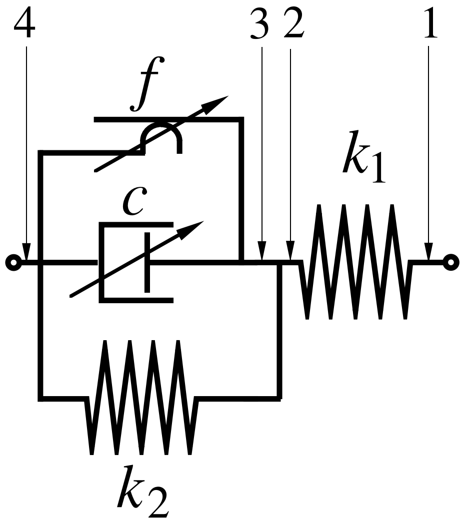

Figure 4. Equivalent model of the MR fluid damper.

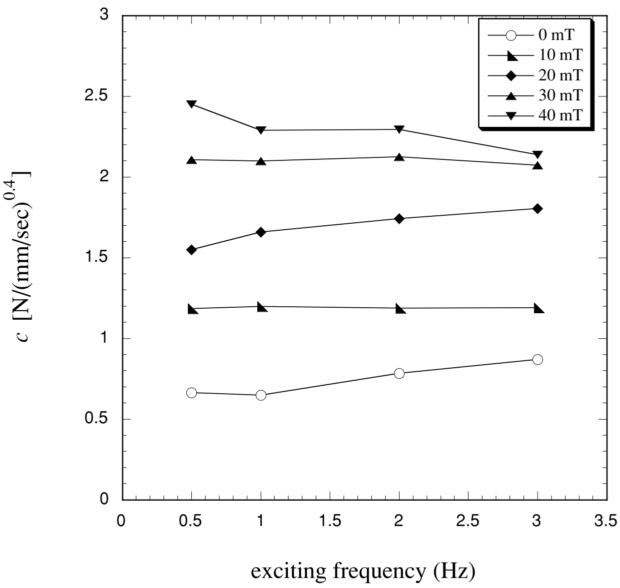

Figure 5. Estimated values of c as a function of input magnetic field and frequency.

of 0 mT. The figure also shows that the 'yielding' load is a monotonically increasing function of the applied magnetic field. These test results show almost the same trend as those of the ER fluid damper of [4]. This fact indicates that the characteristics of the MR fluid are essentially similar to those of the ER fluid, as described in [9].

Based on the test results and the structure of the damper, we propose a mathematical model for the MR fluid damper, which has two spring elements k_1 and k_2, a variable viscous damping element c, and a variable Coulomb-friction element f, as shown in figure 4. The spring constant k_1 reflects the compressibility of the fluid in the chamber. The spring constant k_2 reflects the axial stiffness of the bellows and also includes the spring at the left end of the damper.

In this model, if we assume that the damping force caused by c is proportional to $\dot{e}|\dot{e}|^{n-1}$, the force relation generated by the device is given by

$$c\dot{e}\left|\dot{e}\right|^{n-1} = (g - \hat{f}) \tag{1}$$

$$\hat{f}\begin{Bmatrix} f & \text{when} & f < g \\ g & \text{when} & -f \leqslant g \leqslant f \\ -f & \text{when} & g < -f \end{Bmatrix} \tag{2}$$

where e is the elongation between points 2 and 4 of the damper model. The equation of tensile load g at point 3 of the damper model is given by

$$g = p - k_2 e \tag{3}$$

where p indicates the tensile load on the damper that was measured in the tests. The equation of elongation e also can be derived as

$$e = d - p/k_1 \tag{4}$$

where d indicates the elongation of the damper that was measured in the tests.

We have tried to estimate the values of k_1, k_2, c and f from the equivalent model and test results. The values of k_1 and k_2 can be estimated from the slopes of the plots of the d–p relations as shown in figure 3. When the tensile load g applied to point 3 in figure 4 is less than the frictional force f, only the spring element k_1 elongates because the elongation e between points 3 and 4 in figure 4 is stuck by a larger value of friction f. Therefore, in the high stiffness region in figure 3 we can estimate the value of k_1. When the tensile load g is larger than the frictional force f, both spring elements k_1 and k_2 elongate because e starts to slip. Therefore, $k_1k_2/(k_1 + k_2)$ corresponds to the stiffness in the low stiffness region in figure 3. The values of k_1 and k_2 are thus estimated to be 222.2 N/mm and 30.57 N/mm, respectively.

The values c and f represent the characteristics of the fluid in the bottleneck and were numerically determined so as to minimize a quadratic index J, which is defined as

$$J(c, f) \equiv \sum_{k=1}^{N}(p_k - \tilde{p}_k)^2 \tag{5}$$

where N is the total number of data used for parameter estimation, p is the value measured in the tests and $\tilde{p}$ is the value of p calculated from the measured time history of d, p and the previously estimated values of k_1 and k_2, because the d–p relation can be derived from equations (1)–(4) and $\dot{e} = \dot{d} - \dot{p}/k_1$. The values of c and f for each input magnetic field were estimated from the measured data when the exciting frequencies were 0.5, 1, 2 and 3 Hz.

Figures 5 and 6 show the estimated values of c and f, respectively, as a function of excitation frequency for each input magnetic field H. When the value of n was chosen to be 0.4, the calculated values showed the best agreement with the measured data for all input magnetic fields. The figures show that c and f heavily depend on the applied magnetic field H. They also show that c and f vary slightly at every frequency. These results suggest that c and f are almost independent of frequency.

Figure 7 compares the measured values of p with values of $\tilde{p}$ calculated from the equivalent model of figure 4 with the estimated parameter values shown in figures 5 and 6, where the exciting frequency is 0.5 Hz. The calculated values almost coincide with the measured data for all input magnetic fields.

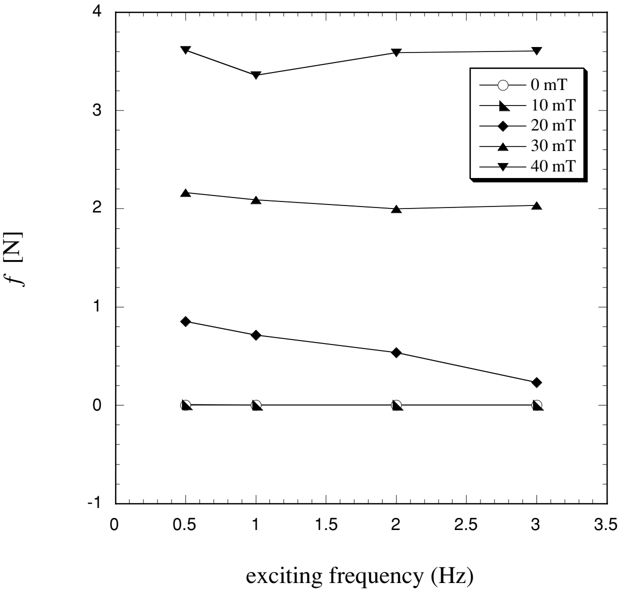

Figure 6. Estimated values of f as a function of input magnetic field and frequency.

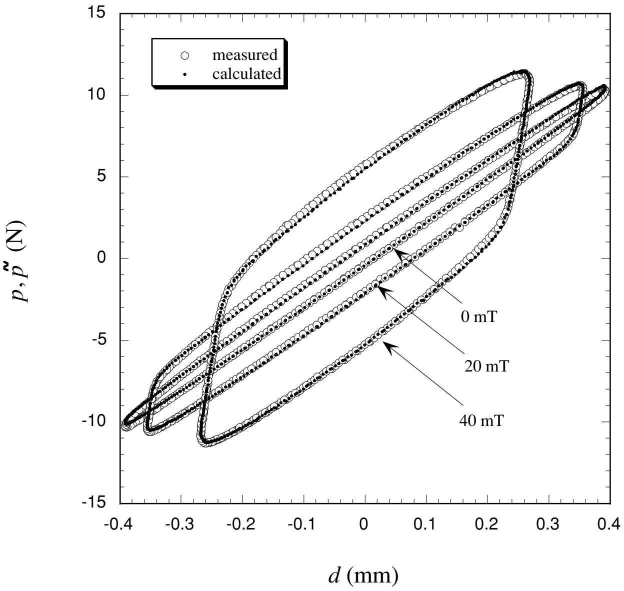

Figure 7. Comparison of measured values of p (exciting frequency = 0.5 Hz) with the values of $\tilde{p}$ numerically calculated from the equivalent model as shown in figure 4.

This fact indicates that the mathematical model predicts the characteristics of the damper very well.

3. Semiactive vibration suppression experiments with MR damper

To investigate whether the MR damper is actually effective for semiactive vibration suppression of truss structures, we performed vibration suppression experiments. Figure 8 shows a block diagram of the vibration suppression experiments. The truss structure is the same as that used in [3] except for the addition of the power supply for controlling

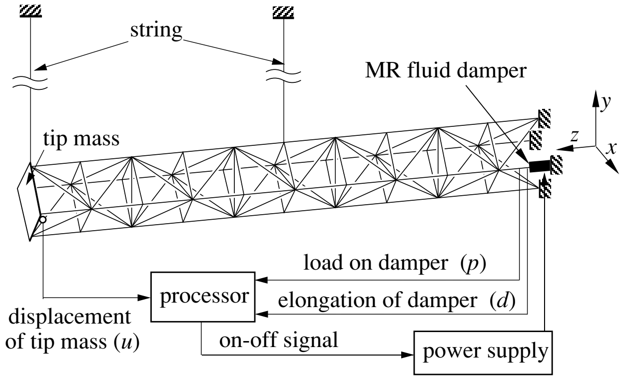

Figure 8. Block diagram for vibration suppression experiments.

the electromagnet. In the experiments, the LQFC-1-b on–off control law of [3, 4] was adopted. This control law is derived from the linear quadratic regulator (LQR) control theory and an equivalent model of the MR damper as shown in figure 4. If we could directly control the value of e, we could use linear control logic based on equation (9) of [4]. In the present system, however, we cannot control the value of e directly. Therefore, we try to control f such that the absolute value of e becomes maximum when the sign of e is the same as e_T (the optimal control value of e obtained from LQR control theory) and such that it becomes minimum otherwise. A possible control logic for this scheme can be implemented as the following control law:

$$\begin{aligned} f &= f_{\min} \quad \text{when} \quad g e_T > 0 \\ f &= f_{\max} \quad \text{when} \quad g e_T < 0. \end{aligned} \tag{6}$$

In [4], this control law is referred to as LQFC-1-b.

In the experiment, we tried to control only the first mode semiactively because, in the case of a space structure, the first mode vibration is dominant. For simplicity, the tip mass displacement u was assumed to be proportional to the first modal displacement. Under this assumption, e_T defined by equation (14) of [4] is proportional to $F_1 u + F_2 \dot{u}$, and g defined by equation (3) can be estimated from equation (4). Therefore, the control law equation (6) was implemented in terms of the measurable variables as follows

$$\begin{aligned} H &= 0 \quad \text{when} \quad \{(1 + k_2/k_1)p - k_2 d\}(F_1 u + F_2 \dot{u}) < 0 \\ H &= H_{\max} \quad \text{when} \quad \{(1 + k_2/k_1)p - k_2 d\}(F_1 u + F_2 \dot{u}) > 0 \end{aligned} \tag{7}$$

Here, the parameter values such as F_1 and F_2 for the LQR controller design were numerically obtained; d and u were measured by using non-contact eddy-current and laser-beam types of displacement sensors, respectively; p was measured by using a strain-gauge type of load cell; and the maximum magnetic field $H_{\max}$ applied to the electromagnet was 40 mT. The power supply for the electromagnet was a dc power supply and it generated a maximum electric current of 2 A.

In the experiments, the tip mass was first displaced in the x-direction by a certain amount, and then it was freed. Subsequently, semiactive control was started during the free vibration of the truss. Figure 9 shows the time histories obtained from the semiactive control using the MR damper.

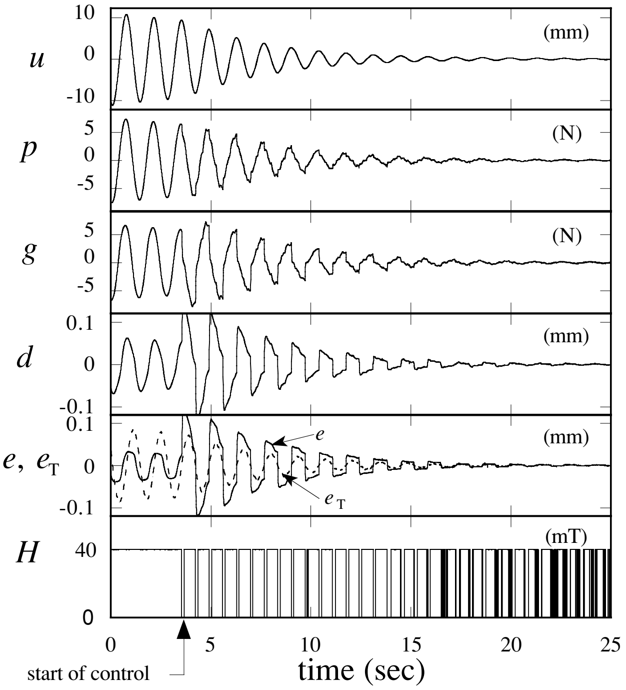

Figure 9. Time histories obtained from the semiactive control of the truss structure with the MR damper.

u indicates the tip mass displacement of the truss. The time histories of g and e were calculated from equations (3) and (4). e_T was calculated from $F_1 u + F_2 \dot{u}$. The figure shows that after the start of the control, the value of e is indirectly controlled such that its absolute value becomes maximum when its sign is the same as e_T and is otherwise minimum, just as the LQFC-1-b control law intends. When the magnetic field applied to the damper decreases, the value of e varies stepwise, and dissipates energy effectively. Consequently, the vibration is suppressed to a low level after starting the control.

To compare the vibration performance of the semiactive system with that of the passive systems, we measured the tip mass displacement u during free decay vibration of the truss under various constant input magnetic fields applied to the MR damper. Figure 10 shows the time history of u for various constant input magnetic fields. The damping in these cases is very slow compared with that shown in figure 9.

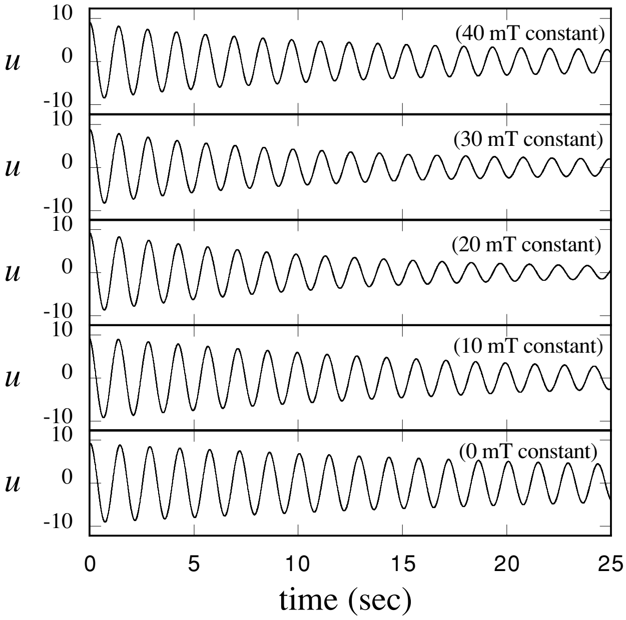

Figure 10. Time histories of u obtained from the passive MR damper under various constant input magnetic fields.

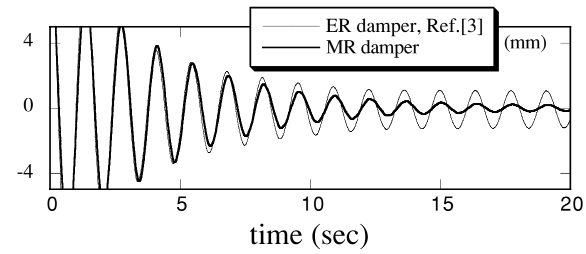

Figure 11. Comparison of the time history of u obtained from experiments using the ER damper with that of the MR damper.

Figure 11 compares the time histories of u obtained from the experiments using the ER damper investigated by Onoda *et al* [3] with that of the MR damper shown in figure 9. For this comparison, the experimental results obtained from the MR and ER dampers are compared under the same condition that amplitudes at the start of the control are almost identical. The MR damper suppresses the vibration to a much smaller level, compared with the ER damper of [3]. Onoda *et al* reported the reason for the degradation of vibration suppression performance of the ER damper as follows. When the vibration was suppressed to a small level, the load on the frictional element of the damper model in figure 4 did not exceed the minimum value of f ($f_{\min}$, the value of f just after turning off the input voltage). As a result, e ceased to respond to turning off the input voltage at 15 s, as shown in figure 11, and the damper ceased to damp. They also reported that this value of $f_{\min}$ ($\approx$1.0 N) is substantially larger than the measured value f ($\approx$0.3 N) when no voltage is applied to the damper. These phenomena may be due to microstructures in the ER fluid that remain around the electrode even after the applied voltage becomes zero. Using an optical microscope, Onoda *et al* [5] observed the behaviour of the microstructure of the ER fluid between the electrodes just after turning off the input voltage. Figure 4 of [5] showed that the chains of particles persisted, even for 2 s after the high voltage to the electrode was turned off. Figure 12 shows the e–g relation obtained from the 16–21 s time history of the semiactive vibration experiments with the ER damper shown in figure 14 of [3]. The figure shows that the damper does not respond to the switching of the input voltage; that is, the frictional element of the mathematical model in figure 4 cannot move because of the relatively large value of $f_{\min}$ even when the input voltages are switched on and off and e ceases to dissipate energy. From this result we can see that the value of $f_{\min}$ is about 1.0 N because the value of g indicates the value of f when the frictional element of the mathematical model in figure 4 becomes stuck. Figure 13 also shows the e–g relation obtained from the 15–20 s time history of the semiactive vibration experiments with the MR damper shown in figure 9. The maximum value of g ($\approx$1.0 N) is almost the same as that of figure 12. The figure shows that

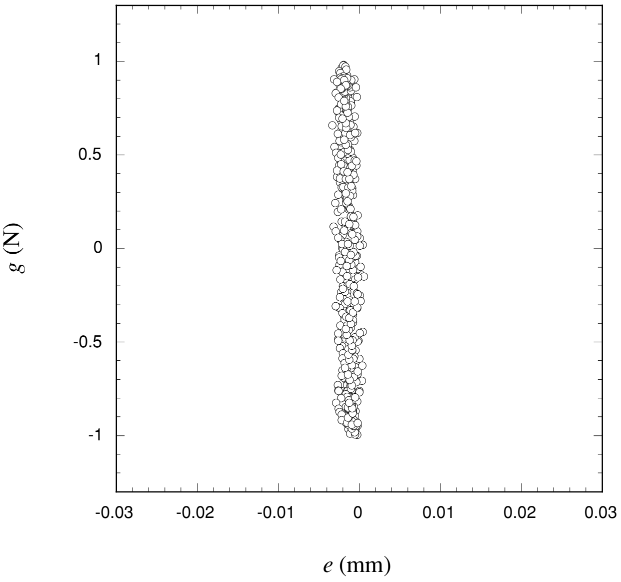

Figure 12. e–g relation obtained from the 16–21s time history of semiactive vibration experiments with the ER damper [3].

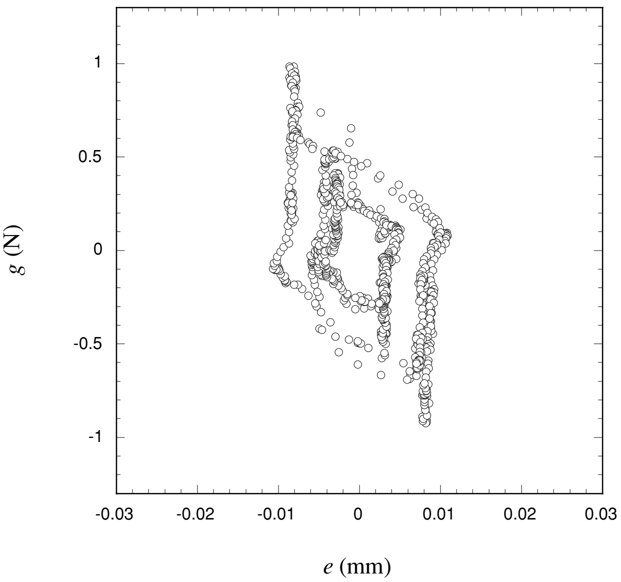

Figure 13. e–g relation obtained from the 15–20 s time history of semiactive vibration experiments with the MR damper.

the value of e continues to respond to switching on and off, and it continues to dissipate energy. As a result, the MR damper suppressed the vibration to a lower level than the ER damper did. Although it is not shown here, the value of e continued to respond to switching on and off even when the value of g decreased to about 0.02N. In other words, the value of $f_{\min}$ of the MR damper is very small. It seems that there was no phenomenon such as microstructures remaining in the fluid just after turning off the control signal, as appeared in the ER damper. Semiactive vibration suppression with ER and MR dampers mainly exploits the variation of friction f. Therefore, $f_{\max}/f_{\min}$ is a key performance parameter. The reason why the MR damper showed a higher performance when the vibration was suppressed to a small level is that the value of $f_{\max}/f_{\min}$ of the MR damper is larger than that of the ER damper.

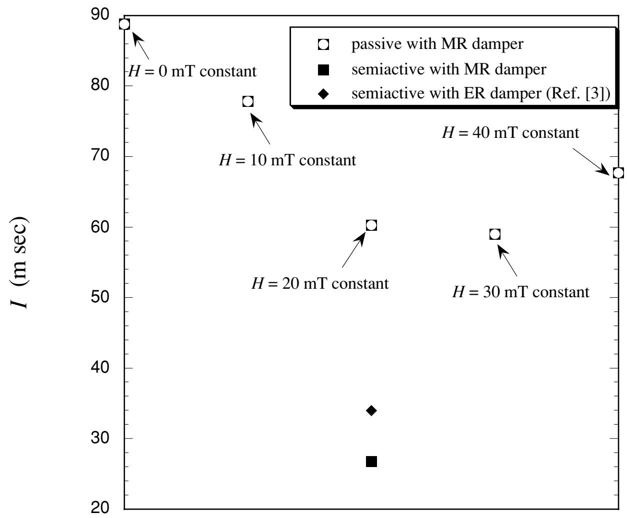

Figure 14. Comparison of the performance of the semiactive MR damper with that of passive systems and the semiactive ER damper.

To compare the vibration suppression performance of the semiactive systems using MR and ER dampers with that of the passive systems, we defined a performance index

$$I = \int_0^{\tau} |u| \, \mathrm{d}t \tag{8}$$

where $\tau = 20$ s. A low value of I indicates high vibration suppression performance. Figure 14 shows the I values calculated from the experimental results. The semiactive system with the MR damper shows much higher performance than the semiactive system with the ER damper [3] and passive systems. From these results, we can see that the semiactive system with the MR fluid damper works nicely for vibration suppression of the actual truss structures.

4. Conclusion

We fabricated a MR fluid damper for semiactive vibration suppression and measured its characteristics in dynamic tests. To investigate the effectiveness of semiactive vibration suppression with the MR damper, we performed semiactive vibration suppression experiments of a cantilevered ten-bay truss beam with the MR damper. The experimental results have shown that the damping performance of the semiactive system with the MR damper is much better than that of passive systems. The experimental results have also shown that the performance of the MR damper is better than that of the ER damper [3] when the vibration is suppressed to a small level.

Acknowledgment

The research described in this paper was supported by a Japan Society for the Promotion of Science (JSPS) postdoctoral fellowship (no P00091).

References

[1] Onoda J, Endo T, Tamaoki H and Watanabe N 1991 Vibration suppression by variable-stiffness members *AIAA J.* **29** 977

[2] Onoda J and Minesugi K 1996 Semi-active vibration suppression by variable damping members *AIAA J.* **34** 335

[3] Onoda J, Oh H-U and Minesugi K 1997 Semi-active vibration suppression of truss structures by electrorheological-fluid *Acta Astronaut. J.* **40** 771

[4] Onoda J, Oh H-U and Minesugi K 1997 Semiactive vibration suppression with electrorheological-fluid dampers *AIAA J.* **35** 1844

[5] Onoda J, Oh H-U and Minesugi K 2000 Improved electrorheological-fluid variable damper for semi-active vibration suppression *AIAA J.* **38** 1736

[6] Oh H-U, Onoda J and Minesugi K 2000 Characteristics of a liquid-crystal type ER-fluid variable damper for semiactive vibration suppression *ASME. J. Vib. Acoust.* **122** 412

[7] Kobori T, Takahashi M, Nasu T, Niwa N and Ogasawara K 1993 Seismic response controlled structure with active variable stiffness system *Earthq. Eng. Struct. Dyn.* **22** 925

[8] Symans M D and Constantinou M C 1997 Seismic testing of a building structure with a semi-active fluid damper control system *Earthq. Eng. Struct. Dyn.* **26** 759

[9] Li Pang, Gopalakrishna M K and Norman M W 1998 Analysis and testing of a linear stroke magnetorheological damper *39th AIAA/ASME/ASCE/AHS/ASC Structural Dynamics, and Materials Conference (Long Beach, CA, Apr 20–25* pp 841–56

[10] Dyke S J, Spencer B F Jr, Sain M K and Carlson J D 1998 An experimental study of MR dampers for seismic protection *Smart Mater. Struct.* **7** 2841

[11] Lee J-K and William W C 1999 Lyapunov semi-active vibration control with an MR fluid actuator *40th AIAA/ASME/ASCE/AHS/ASC Structural Dynamics and Materials Conference (ST. Louis, MO, April 12–15)* pp 2655

[12] Tsuchiya T, Morishita S, Ahn Y-K and Abe Y 1999 Vibration control with a variable-damping mount using MR fluid *Trans. JSME* **640** 83

[13] Spencer B F, Dyke S J, Sain M K and Carlson J D 1997 Phenomenological model for magnetorheological dampers *J. Eng. Mech.* **123** 83